

High-Yield Preparation of Uniform Cobalt Hydroxide and Oxide Nanoplatelets and Their Characterization

Yanglong Hou,[†] Hiroshi Kondoh,[†] Masatsugu Shimojo,[†] Toshihiro Kogure,[‡] and Toshiaki Ohta^{*†}

Departments of Chemistry and of Earth and Planetary Science, School of Science, The University of Tokyo, Tokyo 113-0033, Japan

Received: April 23, 2005; In Final Form: August 22, 2005

Cobalt hydroxide nanoplatelets with a uniform hexagonal shape were prepared in high yield (~95%) by a facile hydrothermal route in the presence of poly(vinylpyrrolidone). This method provides a simple, low-cost, and large-scale route to produce β -cobalt hydroxide nanoplatelets with an average diameter of 280 nm and a thickness of ca. 26 nm which show a predominant well-crystalline hexagonal brucite-like phase. Their thermal decomposition produced anisotropic nanoplatelets of cobalt oxides (CoO and Co₃O₄) under designed temperatures. The products were characterized by transmission electronic microscopy, selected-area electron diffraction, Fourier transform infrared spectroscopy, differential scanning calorimetric, and thermogravimetric analysis. The magnetic properties of the products were investigated by a superconducting quantum interference device magnetometer. Co₃O₄ nanoplatelets exhibit a superparamagnetic behavior, and they might be a promising material to study the magnetic tunneling effect as anisotropic nanostructures.

Introduction

Low-dimensional nanoscale materials have attracted much attention in the development of novel optical, electronic, magnetic, and catalytic materials. Many one-dimensional (1D) nanoscale materials such as nanotubes, nanobelts, nanorods, and nanowires have been prepared by different approaches which can be classified into the following strategies.^{1,2} First, the growth of 1D nanoscale materials is achieved in a hard template with well-confined structures, such as alumina, silica, block polymer, mica, and membranes.^{3,4} Second, soft templates are used to produce 1D nanoscale materials.^{5,6} Generally, in this process, surfactants are applied to stabilize the surface of nanonuclei and kinetically control the growth rates of various facets of nuclei. Third, the intrinsic structures are used to form 1D nanostructures.^{7,8} Usually, the materials with hexagonal structure are favored to form 1D nanostructures under a suitable reaction condition. Fourth, vapor–liquid–solid (VLS) growth has been employed to prepare 1D nanostructures.^{9–11} Recently, it was found that the low-temperature process based on one or more strategies described above is more promising to prepare 1D nanoscale materials. For instance, Ag, Pb, and Pt nanowires have been synthesized by the polyol process without any template.¹² A number of nanosized materials have also been produced by the solvothermal approach.^{13–16} These methods have some potential advantages, such as low cost, high purity, and large-scale production. Apart from wire and tube structures, other anisotropic nanostructures including nanocubes,^{17,18} nanoprisms,¹⁹ nanotetrapods,²⁰ and nanoplatelets or nanosheets^{21–23} have been the focus of intensive research for potential applications in nanoelectronics, data storage, and catalysis. Compared with those on nanorods or nanowires, there have been few

reports on nanoplatelets or nanosheets of hydroxides due to the lack of knowledge on their synthesis.²⁴

Cobalt hydroxides can be used as additives to improve the electrochemical activity of alkaline secondary batteries²⁵ and the tribological property of lubricating oils.²⁶ Cobalt hydroxide films show catalytic and reversible electrochromic properties.^{27,28} In particular, organic groups have been incorporated into the interlayer region of cobalt hydroxides to form organic magnetic materials.²⁹ Several approaches have been employed to prepare nanoplatelets.³⁰ For example, Zeng's group reported the ligand-mediated synthesis of brucite-like cobalt hydroxide nanorods/platelets consisting of linear arrays of assembled "butterflies".³¹

The β -Co(OH)₂ bulk crystal has a hexagonal structure with space group $p\bar{3}m1$ and lattice constants of $a = 3.191 \text{ \AA}$ and $c = 4.664 \text{ \AA}$ (JCPDS file no. 30-443). This is a layered compound composed of a Co layer sandwiched by two O layers. Cobalt hydroxides prefer to grow into nanoplatelets due to their intrinsic lamellar structures. It is desirable to conduct further structural analysis for both of these species to understand the correlation between the geometric and magnetic structures.

Spinel Co₃O₄ is an important P-type semiconductor due to its potential applications in ceramic pigments, solid-state sensors, energy storage as intercalation compounds, rotatable magnets, heterogeneous catalysts, and electrochromic devices.^{32–35} Especially, it is very useful to prepare anisotropic antiferromagnetic nanostructures for studying the magnetic properties as a function of geometric structure.³⁴ Some efforts have been focused on the synthesis of cobalt oxide nanocubes,³² nanorods,³⁶ or nanotubes.³⁷ Here, we employed a facile solvothermal approach to synthesize Co(OH)₂ nanoplatelets. Cobalt oxide nanoplatelets were readily obtained by thermal decomposition of Co(OH)₂ nanoplatelets. The magnetic properties of cobalt oxide nanoplatelets were also investigated.

* To whom correspondence should be addressed. Fax: 81 3 3812 1896. E-mail: ohta@chem.s.u-tokyo.ac.jp.

[†] Department of Chemistry.

[‡] Department of Earth and Planetary Science.

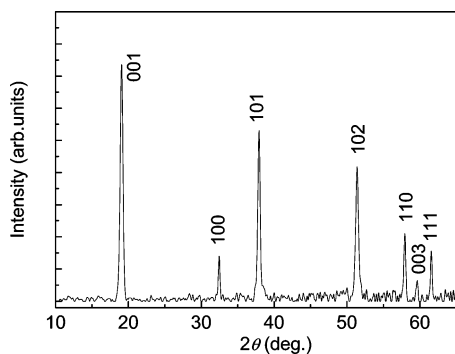


Figure 1. XRD pattern of the as-prepared product (sample A). Indexing is based on the structure of β -cobalt hydroxides (JCPDS file no. 30-443).

Experimental Section

Cobalt hydroxide nanoplatelets were prepared by the precipitation and hydrothermal process. In a typical procedure, 2.5 g of $\text{Co}(\text{NO}_3)_2 \cdot 6\text{H}_2\text{O}$ and a designed amount (from 3.3 to 0 g) of poly(vinylpyrrolidone) (PVP) were dissolved in a 20 mL mixture of ethanol and distilled water with a 1:1 volume ratio in a three-neck flask. The solution was bubbled with Ar for 30 min, and 50 mL of a 0.4 M NaOH aqueous solution was slowly added, taking 1.5 h. This caused a color evolution from blue to red-pink, indicating the phase change from the α to β phase of $\text{Co}(\text{OH})_2$. The reaction suspension was quickly transferred into an autoclave with a Teflon cup. The autoclave was heated to 120 °C and maintained at that temperature for 6 h. After the autoclave was cooled to room temperature naturally, red-pink precipitates were collected by centrifugation. By washing with acetone and distilled water sequentially, possible excess surfactants and byproducts could be removed from the products. The red-pink powders then were dried in a vacuum at 60 °C for 5 h for further characterization.

Oxide nanoplatelets were obtained by thermal decomposition of cobalt hydroxide nanoplatelets. Heating $\text{Co}(\text{OH})_2$ nanoplatelets at 220 °C for 4 h under atmospheric Ar produced CoO , while heating them at 450 °C for 5 h in air produced Co_3O_4 . Gray-black powders thus obtained were collected for characterization.

Powder X-ray diffraction (XRD) patterns of the samples were measured with a Rigaku Mini diffractometer with $\text{Cu K}\alpha$ radiation ($\lambda = 0.15418$ nm). Transmission electron microscopy (TEM) images were obtained with a Hitachi HF-2000 electron microscope. Infrared spectra of the samples formed in KBr platelets were recorded with a Jasco FT/IR 420 spectrometer to confirm the formation of $\text{Co}(\text{OH})_2$. The thermogravimetric (TG) analysis and differential scanning calorimetric (DSC) analysis were carried out in air with a Rigaku Thermplus TG8120 with a heating rate of 5 °C/min. Magnetic studies were conducted on cobalt hydroxide and oxide nanoplatelets by using a superconducting quantum interference device (SQUID) magnetometer (Quantum Design Co. Ltd.).

Results and Discussion

Characterization of Cobalt Hydroxide Nanoplatelets. Structural information on the products was obtained by XRD measurement. Figure 1 shows the XRD pattern of a sample stabilized with 3.3 g of PVP, which is denoted hereafter as sample A. It exhibits a predominant well-crystalline brucite-like phase (JCPDS file no. 30-443) in which the 2θ scan has peaks at 19.0°, 32.4°, and 37.9°, corresponding to the (001), (100), and (101) diffractions. The FTIR spectrum of sample A

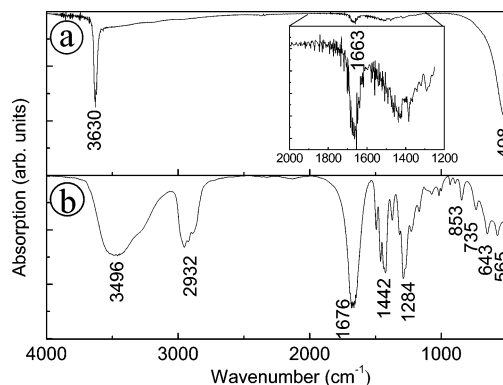


Figure 2. FTIR spectra from (a) the as-prepared cobalt hydroxide nanoplatelets (sample A) and (b) PVP.

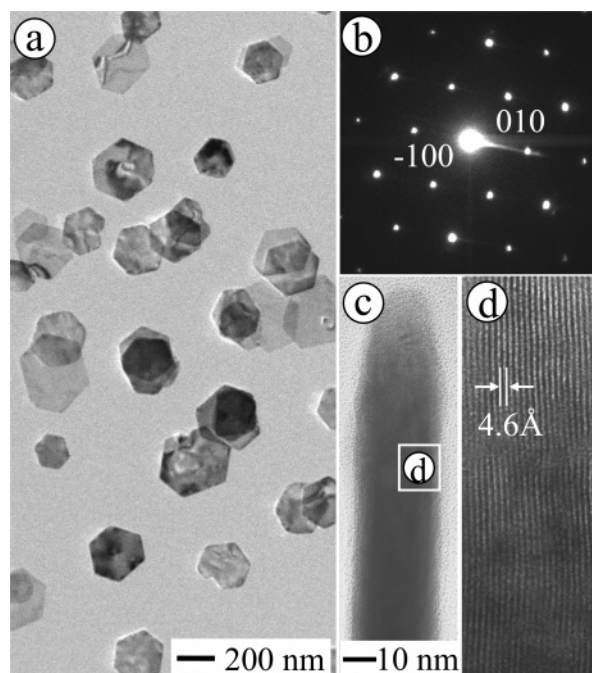


Figure 3. TEM images of the as-prepared β -cobalt hydroxide nanoplatelets (sample A): (a) survey, (b) a typical SAED pattern, (c) side view, and (d) HRTEM image of an area selected in (c).

is compared with that of PVP in Figure 2. A sharp peak observed at 3630 cm^{-1} is assigned to the hydroxyl group in the brucite-like structure enhanced due to high basicity. No peak appears at 1384 cm^{-1} , which is a typical absorbance of nitrate anions,^{30,31} indicating no intercalation of nitrate anions in the sample. The peak at 1663 cm^{-1} in sample A might correspond to the peak at 1676 cm^{-1} of PVP with a slight shift, indicating chemical bond formation between PVP and the nanoplatelets. The peaks in the region of 496–540 cm^{-1} can be assigned to metal–oxygen vibrations and metal–OH bending vibrations in the brucite-like octahedron sheets.³⁰ Thus, the FTIR measurement also confirms the formation of a brucite-like structure.

The morphology of the products was characterized by TEM. As shown in Figure 3a, one can see that cobalt hydroxides are well-defined hexagonal platelets with a size of about 280 nm, showing a relatively narrow size distribution (Supporting Information Figure SI-1). Figure 3b is a typical SAED pattern, exhibiting the hexagonal structures of brucite-like β -cobalt hydroxides. The side-view image (Figure 3c) indicates that the thickness of the plates is ca. 26 nm. As shown in Figure 3d, the HRTEM image confirms the layer structure with a lattice

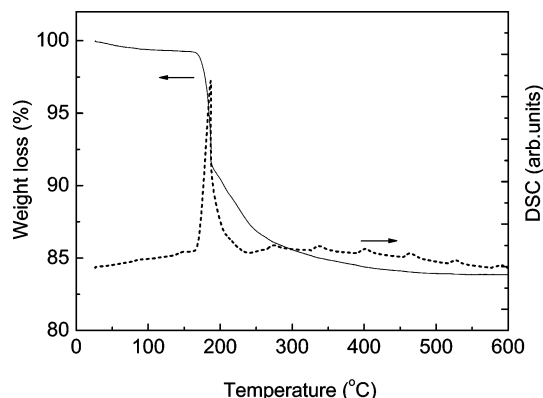


Figure 4. TG curve (solid line) and DSC plots (dashed line) of as-prepared cobalt hydroxide nanoplatelets (sample A).

spacing of 4.6 Å, in accordance with the (001) plane of brucite-like β -cobalt hydroxides.

The thermal behavior of β -cobalt hydroxides was investigated with TG and DSC measurements. Figure 4 shows a typical TG analysis curve of cobalt hydroxide nanoplatelets coated with surfactants. The gradual mass loss at lower temperatures can be attributed to evaporation of the surfactants attached to the nanoplatelet surfaces. The dominant mass loss profile exhibits a well-defined decrease over a temperature range of 165–350 °C with an inflection point at about 180 °C. The total mass loss was estimated to be $\sim 17\%$, slightly lower than the theoretical value (19.4%) calculated from the thermal decomposition of cobalt hydroxides: $\text{Co}(\text{OH})_2 \rightarrow \text{CoO} + \text{H}_2\text{O}$. This suggests incomplete decomposition even around 350 °C for a few minutes. The DSC curve shows an endothermic peak at 185 °C, corresponding to the dominant mass loss. Similar behavior was also observed in the cases of nickel and magnesium hydroxides.³⁰

Next, we investigated the influence of PVP concentration on the morphology of the products. Samples A and B are products stabilized with 3.3 and 1.5 g of PVP, respectively, while sample C was prepared without PVP. XRD measurements indicate that all three of these pink-red colored samples exhibit a typical brucite-like $\text{Co}(\text{OH})_2$ phase (see Supporting Information Figure SI-2). However, TEM observations show that samples B and C are composed of semiplatelets with irregular morphologies and some cracks (Supporting Information Figure SI-3). We can conclude that the use of PVP is a key to achieve a high yield ($\sim 95\%$) of uniform nanoplatelet structures and the amount of PVP affects the morphology of the products.

Characterization of Cobalt Oxide Nanoplatelets. Generally, the formation of cobalt oxide nanoplatelets is sensitively dependent on the reaction conditions and intrinsic structures. We employed single-crystalline cobalt hydroxide nanoplatelets as the precursors to prepare cobalt oxide nanoplatelets. On the basis of the results of the TG analysis, we adopted the condition of heating at 220 °C under atmospheric Ar to convert $\text{Co}(\text{OH})_2$ completely to CoO and that of heating at 450 °C in air to prepare Co_3O_4 . Figure 5a shows the morphology of the sample annealed at 220 °C for 4 h under Ar, where one can see that the sample sustains platelet structures. The HRTEM image (Figure 5b) indicates a highly crystalline character with a lattice spacing of 2.4 Å, corresponding to the value of the (111) plane of the CoO phase. To investigate the structure of the sample further, the XRD pattern was analyzed, as shown in Figure 5c, where all reflection peaks at (111), (200), and (220) can be indexed to the peaks of the CoO phase. The lattice constant ($a = 4.26$ Å) is in good agreement with bulk CoO (from Wako Chemicals,

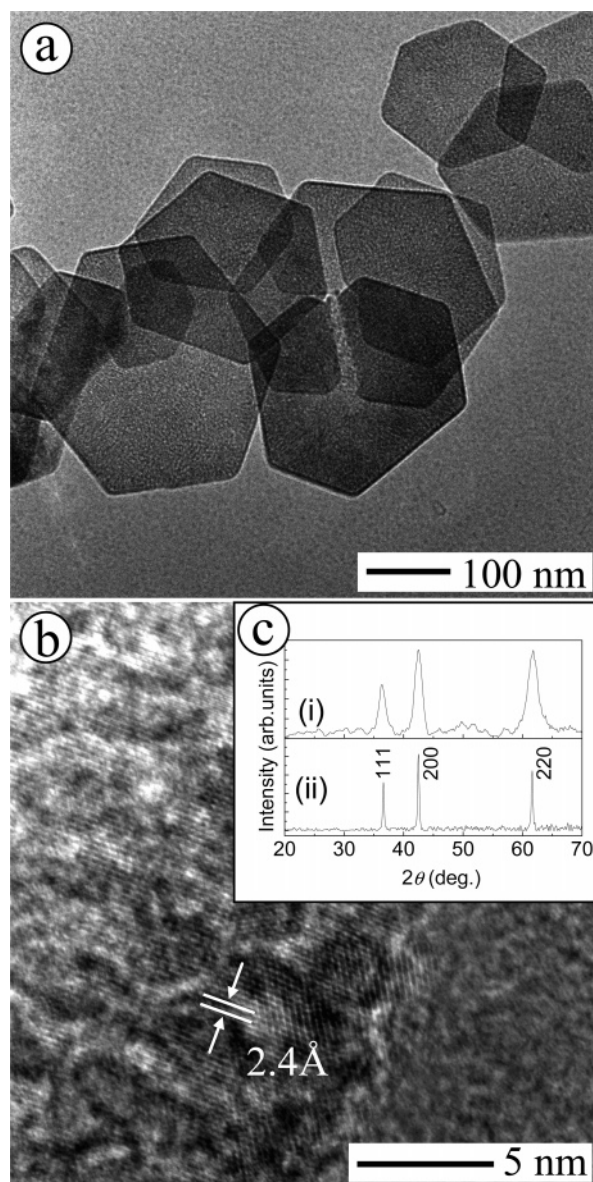


Figure 5. (a) TEM image of the CoO nanoplatelets. The inset is an SAED pattern. (b) A typical HRTEM image of the CoO nanoplatelets in (a). The lattice spacing of 2.4 Å consists with the (111) plane in bulk CoO. (c) XRD patterns from (i) the CoO nanoplatelets and (ii) bulk CoO (Wako Chemicals Ltd.). Indexing is based on the structure of CoO, JCPDS file no. 48-1719.

space group $Fm\bar{3}m$, JCPDS file no. 48-1719). No peaks due to hydroxides were observed, indicating the complete decomposition of hydroxides under an inert Ar atmosphere. After being annealed at 450 °C for 5 h in air, the sample was characterized by TEM and X-ray diffraction. As shown in Figure 6a, the sample exhibits platelet morphology although there are some cracks. The HRTEM image shows a well-defined crystalline structure with a lattice spacing of 4.6 Å, corresponding to the value of the (111) plane of the Co_3O_4 phase. The inset in Figure 6b is the fast Fourier transform (FFT) pattern of the sample. All reflections of XRD patterns in Figure 5c are indexed to the Co_3O_4 phase (space group $Fd\bar{3}m$, JCPDS file no. 78-1970), consistent with the indices of bulk Co_3O_4 (from Wako Chemicals).

Magnetic Properties of the Products. Both cobalt hydroxides and CoO nanoplatelets have a typical antiferromagnetic behavior. It was noted that Co_3O_4 nanoplatelets show superparamagnetic behavior. The temperature dependences of mag-

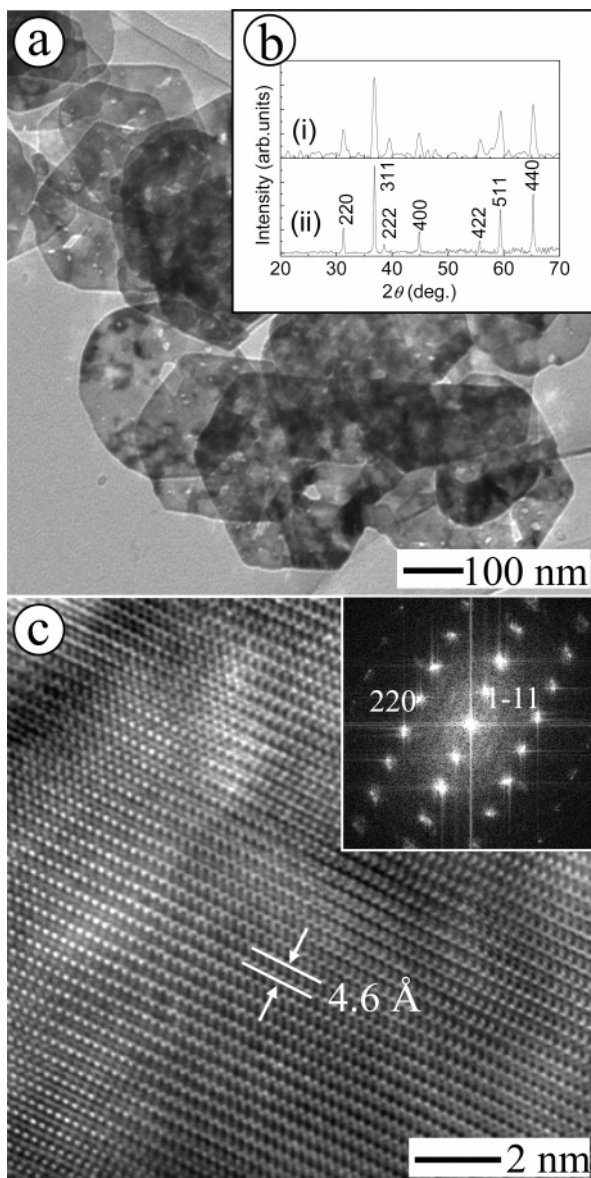


Figure 6. (a) TEM image of the Co_3O_4 nanoplatelets. (b) XRD patterns from (i) the Co_3O_4 nanoplatelets and (ii) bulk Co_3O_4 (Wako Chemicals Ltd.). Indexing is based on the structure of Co_3O_4 , JCPDS file no. 78-1970. (c) A typical HRTEM image of the Co_3O_4 nanoplatelets in (a). The inset is the Fourier transform pattern.

netization of the Co_3O_4 nanoplatelets in zero-field-cooled (ZFC) and field-cooled (FC) conditions are shown in Figure 7. A sharp maximum is observed at around 35 K (blocking temperature T_B), which is expected to be the freezing temperature of residual spin moments. Above 35 K, both the ZFC and FC magnetization curves decrease with temperature. The plots of χ^{-1} as a function of temperature show a linear feature, indicating that the magnetization obeys the Curie–Weiss law with a Θ value of about 30 K. From the Curie constant, the value of the effective magnetic moment per ion in the paramagnetic state could be estimated to be $4.2 \mu_B$. The superparamagnetic behavior might be due to the blocking effect of the resultant spins caused by incompenation for Co_3O_4 nanocrystals,³⁴ which is in contrast with the behavior of bulk antiferromagnetic Co_3O_4 . We found a small hysteresis loop on the magnetization curve measured at 2 K (< 35 K), although the magnetization curve shows no hysteresis at room temperature, as shown in Figure 8. The field derivative of the magnetization has been used to detect the resonant spin tunneling in Mn-12 molecules and ferriton.^{38,39}

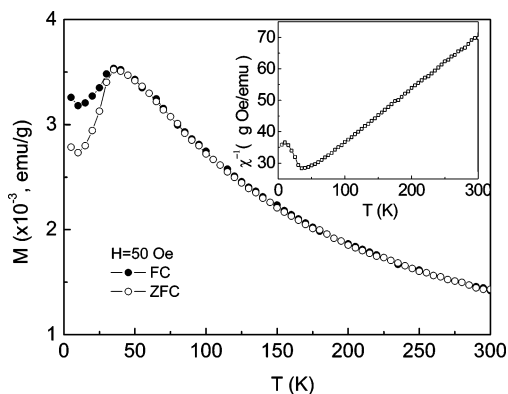


Figure 7. ZFC and FC magnetization curves of the Co_3O_4 nanoplatelets in an applied field of 50 Oe.

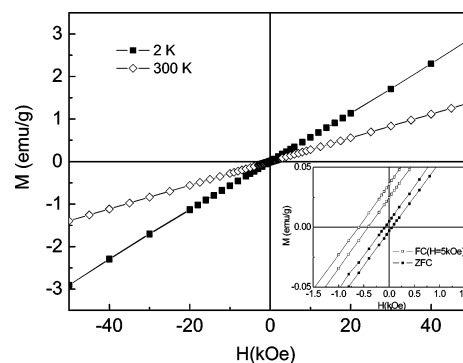


Figure 8. Hysteresis loops of the Co_3O_4 nanoplatelets, measured at 2 and 300 K after zero-field cooling. Enlarged loops at 2 K after field cooling ($H = 5$ kOe) are shown in the inset.

As expected, dM/dH has a sharp peak at $H = 0$, which is similar to the behavior observed in manganese-12 acetate and ferriton. The shifted hysteresis loop was observed after a field cooling. The central portions of the ZFC and FC hysteresis loops are shown in the inset. The FC loop is slightly broadened and shifted along the direction of the applied field, with an exchange field of $H_e = 500$ Oe at 2 K, indicating the presence of unidirectional exchange anisotropy.⁴⁰

Conclusions

We presented a high-yield synthesis of uniform cobalt hydroxide and oxide nanoplatelets with a size of 280 nm and a thickness of ca. 26 nm via a facile hydrothermal route. The use of PVP as a stabilizer is a key to prepare the uniform nanoplatelet structures, and its amount affects the morphology of the products. Thermal decomposition was employed to produce anisotropic nanoplatelets of cobalt oxides. Co_3O_4 nanoplatelets exhibit superparamagnetic behavior and can be used for the study of magnetic tunneling as anisotropic nanostructures.

Acknowledgment. This work was supported by the Japan Society for the Promotion of Science (JSPS) and the 21st Century COE Program from the Ministry of Education, Culture, Sports, Science and Technology.

Supporting Information Available: Size distribution of sample A (Figure SI-1), XRD patterns of the as-prepared products prepared in the presence of different amounts of PVP (Figure SI-2), and TEM images of samples B and C (Figure SI-3). This material is available free of charge via the Internet at <http://pubs.acs.org>.

References and Notes

- (1) (a) Xia, Y.; Yang, P.; Sun, Y.; Wu, Y.; Mayers, B.; Gates, B.; Yin, Y.; Kim, F.; Yan, H. *Adv. Mater.* **2003**, *15*, 353. (b) El-Sayed, M. A. *Acc. Chem. Res.* **2001**, *34*, 257. (c) Hu, J.; Odom, T. W.; Lieber, C. M. *Acc. Chem. Res.* **1999**, *32*, 435.
- (2) Milliron, D. J.; Hughes, S. M.; Cui, Y.; Manna, L.; Li, J.; Wang, L. W.; Alivisatos, A. P. *Nature* **2004**, *430*, 190.
- (3) (a) Thurn-Albert, T.; Schotter, J.; Kästle, G. A.; Emley, N.; Shiibaushi, T.; Krusin-Elbaum, L.; Guarini, K.; Black, C. T.; Tuominen, M. T.; Russell, T. P. *Science* **2000**, *290*, 2126. (b) Zhang, L.; Dutta, A. K.; Jarero, G.; Stroev, P. *Langmuir* **2000**, *16*, 7095.
- (4) Wirtz, M.; Martin, C. R. *Adv. Mater.* **2003**, *15*, 445.
- (5) Park, S.-J.; Kim, S.; Lee, S.; Khim, Z.; Char, K.; Hyeon, T. *J. Am. Chem. Soc.* **2000**, *122*, 8581.
- (6) Peng, X.; Wickham, J.; Alivisatos, A. P. *J. Am. Chem. Soc.* **1998**, *120*, 5343.
- (7) Ma, Y.; Qi, L.; Ma, J.; Cheng, H. *Adv. Mater.* **2004**, *16*, 1023.
- (8) Liu, B.; Zeng, H. C. *J. Am. Chem. Soc.* **2003**, *125*, 4430.
- (9) Wang, Z. L. *Annu. Rev. Phys. Chem.* **2004**, *55*, 159.
- (10) Liu, J.; Fan, S.; Dai, H. *Mater. Res. Soc. Bull.* **2004**, *29*, 244.
- (11) Hu, J.-Q.; Li, Q.; Meng, X.-M.; Lee, C.-S.; Lee, S.-T. *Adv. Mater.* **2002**, *14*, 1195.
- (12) (a) Sun, Y.; Xia, Y. *Adv. Mater.* **2002**, *14*, 833. (b) Wang, Y.; Herricks, T.; Xia, Y. *Nano Lett.* **2003**, *3*, 1163. (c) Chem, J.; Herricks, T.; Geissler, M.; Xia, Y. *J. Am. Chem. Soc.* **2004**, *126*, 10854.
- (13) (a) Liu, Z.; Liang, J.; Li, S.; Peng, S.; Qian, Y. *Chem.—Eur. J.* **2004**, *10*, 634. (b) Yu, S. H.; Yoshimura, M. *Adv. Mater.* **2002**, *14*, 296.
- (14) Wang, X.; Li, Y. D. *Chem.—Eur. J.* **2003**, *9*, 5627.
- (15) (a) Hou, Y.; Kondoh, H.; Shimojo, M.; Sako, E. O.; Ozaki, N.; Kogure, T.; Ohta, T. *J. Phys. Chem. B* **2005**, *109*, 4845. (b) Hou, Y.; Yu, J.; Gao, S. *J. Mater. Chem.* **2003**, *13*, 1983. (c) Hou, Y.; Gao, S. *J. Alloys Compd.* **2004**, *365*, 112. (d) Hou, Y.; Kondoh, H. T.; Ohta, T. *Chem. Mater.* **2005**, *17*, 3994.
- (16) Guo, Q.; Xie, Y.; Wang, X.; Zhang, S.; Hou, T.; Lv, S. *Chem. Commun.* **2004**, *15*, 26.
- (17) (a) Sun, Y.; Xia, Y. *Science* **2002**, *298*, 2176. (b) Dumestre, F.; Chaudret, B.; Amiens, C.; Renaud, P.; Fejes, P. *Science* **2004**, *303*, 821. (c) Kim, F.; Connor, S.; Dong, H.; Kuykendall, T.; Yang, P. *Angew. Chem., Int. Ed.* **2004**, *43*, 3673.
- (18) (a) Gou, L.; Murphy, C. J. *Nano Lett.* **2003**, *3*, 231. (b) Feng, J.; Zeng, H. C. *Chem. Mater.* **2003**, *15*, 2829.
- (19) (a) Jin, R.; Cao, Y. C.; Hao, E.; Métraux, G. S.; Schatz, G. C.; Mirkin, C. A. *Nature* **2003**, *425*, 487. (b) Callegari, A.; Tonti, D.; Chergui, M. *Nano Lett.* **2003**, *3*, 1565.
- (20) Wang, D.; Lieber, C. M. *Nat. Mater.* **2003**, *2*, 355.
- (21) (a) Gibson, C. O.; Putzer, K. *Science* **1995**, *267*, 2338. (b) Puentes, V. F.; Zanchet, D.; Erdonmez, C. K.; Alivisatos, A. P. *J. Am. Chem. Soc.* **2002**, *124*, 12784.
- (22) (a) Maillard, M.; Giorgio, S.; Pileni, M.-P. *Adv. Mater.* **2002**, *14*, 1084. (b) Maillard, M.; Huang, P.; Brus, L. *Nano Lett.* **2003**, *3*, 1611.
- (23) Dai, Z. R.; Pan, Z. W.; Wang, Z. L. *J. Am. Chem. Soc.* **2002**, *124*, 8673.
- (24) (a) Yu, J. C.; Xu, A.; Zhang, L.; Song, R.; Wu, L. *J. Phys. Chem. B* **2004**, *108*, 64. (b) Liang, Z. H.; Zhu, Y. J.; Hu, X. L. *J. Phys. Chem. B* **2004**, *108*, 3488. (c) Ichiiyanagi, Y.; Kondoh, H.; Yokoyama, T.; Okamoto, K.; Nagai, K.; Ohta, T. *Chem. Phys. Lett.* **2003**, *379*, 345.
- (25) (a) Watanabe, K.; Kikukawa, T.; Kumagai, N. *J. Appl. Electrochem.* **1995**, *25*, 219. (b) Elumalai, P.; Vasani, H. N.; Munichandraiah, N. *J. Power Sources* **2001**, *93*, 201.
- (26) Chen, G. X.; Hu, Z. S.; Dong, J. X.; Wang, L. G.; Peng, Y.; He, T.; Lai, R. *Lu. Eng.* **2001**, *57*, 36.
- (27) Dinamani, M.; Kamath, P. V. *J. Appl. Electrochem.* **2000**, *305*, 1157.
- (28) Jozer, N.; Chen, D. G.; Buyuklimanli, T. *Sol. Energy Mater. Sol. Cells* **1998**, *52*, 223.
- (29) Kurmoo, M. *Chem. Mater.* **1999**, *11*, 3370.
- (30) (a) Zhu, Y.; Li, H.; Kottypin, Y.; Gedanken, A. *J. Mater. Chem.* **2002**, *12*, 729. (b) Pralong, V.; Delahaye-Vidal, A.; Beaudoin, B.; Gerand, B.; Tarascon, J. M. *J. Mater. Chem.* **1999**, *9*, 955.
- (31) (a) Xu, Z. P.; Zeng, H. C. *Chem. Mater.* **1999**, *11*, 67. (b) Xu, Z. P.; Zeng, H. C. *J. Mater. Chem.* **1998**, *8*, 2499. (c) Sampanthar, J. T.; Zeng, H. C. *J. Am. Chem. Soc.* **2002**, *124*, 6668.
- (32) (a) Xu, R.; Zeng, H. C. *Langmuir* **2004**, *20*, 9780. (b) Xu, R.; Zeng, H. C. *J. Phys. Chem. B* **2003**, *107*, 926.
- (33) He, T.; Chen, D.; Jiao, X.; Xu, Y.; Gu, Y. *Langmuir* **2004**, *20*, 8408.
- (34) (a) Takada, S.; Fujii, M.; Kohiki, S. *Nano Lett.* **2001**, *1*, 379. (b) Makhlof, S. A. *J. Magn. Magn. Mater.* **2002**, *246*, 184.
- (35) Barreca, D.; Massignan, C.; Daolio, S.; Fabrizio, M.; Piccirillo, C.; Armelao, L.; Tondello, E. *Chem. Mater.* **2001**, *13*, 588.
- (36) (a) Lakshmi, B. B.; Patrissi, C. J.; Martin, C. R. *Chem. Mater.* **1997**, *9*, 2544. (b) Liu, Y.; Wang, G.; Xu, C.; Wang, W. *Chem. Commun.* **2002**, 1486.
- (37) Shi, X. S.; Han, S.; Sanedrin, R. J.; Zhou, F.; Selke, M. *Chem. Mater.* **2002**, *14*, 1897.
- (38) Awschalom, D. D.; Smyth, J. F.; Grinstein, G.; DiVincenzo, D. P.; Loss, D. *Phys. Rev. Lett.* **1992**, *68*, 3092.
- (39) Tejada, J.; Zhang, X. X.; del Barco, E.; Hernández, J. M. *Phys. Rev. Lett.* **1997**, *79*, 1754.
- (40) Meiklejohn, W. H. *J. Appl. Phys.* **1962**, *33*, 1328.